AIP | Applied Physics Letters

Step tunneling enhanced asymmetry in asymmetric electrode metal-insulator-insulator-metal tunnel diodes

N. Alimardani and J. F. Conley

Citation: Appl. Phys. Lett. **102**, 143501 (2013); doi: 10.1063/1.4799964
View online: http://dx.doi.org/10.1063/1.4799964
View Table of Contents: http://apl.aip.org/resource/1/APPLAB/v102/i14
Published by the American Institute of Physics.

Step tunneling enhanced asymmetry in asymmetric electrode metal-insulator-insulator-metal tunnel diodes

N. Alimardani and J. F. Conley, Jr.[a)]
School of Electrical Engineering and Computer Science, Oregon State University, Corvallis, Oregon 97331, USA

(Received 28 October 2012; accepted 22 March 2013; published online 9 April 2013)

The impact of nanolaminate insulator tunnel barriers on asymmetric metal workfunction metal-insulator-insulator-metal (MIIM) devices is investigated. We demonstrate experimentally that bilayer insulators introduce additional asymmetry and can be arranged to either enhance or oppose the asymmetry induced by the asymmetric workfunction electrodes. It is also shown that step tunneling can dominate the I-V asymmetry of M_1IIM_2 diodes. By combining bilayer tunnel barriers with the standard approach of asymmetric metal electrodes, we are able to achieve low voltage asymmetry and non-linearity exceeding both that of standard single layer asymmetric electrode metal-insulator-metal devices as well as symmetric electrode $M_1I_1I_2M_1$ devices. © *2013 American Institute of Physics*. [http://dx.doi.org/10.1063/1.4799964]

Thin film metal-insulator-metal (MIM) tunnel devices have seen renewed interest for high speed applications[1–3] such as infrared (IR) detectors,[4–6] optical rectennas for IR energy harvesting,[7–9] and hot electron transistors,[10] as well as for macroelectronic applications such as backplanes for liquid-crystal displays (LCDs).[11,12] For many of these applications, highly asymmetric and non-linear current vs. voltage (I-V) behavior at low applied voltages is desired. The standard approach to achieving asymmetric I-V characteristics in tunnel devices is to use metal electrodes with different workfunctions (Φ_M) to make M_1IM_2 diodes where $\Phi_{M1} \neq \Phi_{M2}$, to produce a built-in voltage, $V_{bi} = (\Phi_{M1} - \Phi_{M2})/e$ (where e is the electronic charge) across the tunnel barrier.[13,14] However, the amount of asymmetry achievable using this approach is limited by the $\Delta\Phi_M$ that can be obtained using practical electrodes. An alternative approach to achieving asymmetric and non-linear operation involves engineering of the tunnel barrier so that electrons tunneling from one metal electrode to the other are presented with a different barrier shape depending on the direction of tunneling/applied bias polarity.[15] Formation of an asymmetric tunnel barrier can be accomplished using nanolaminate pairs of insulators, each having different band-gaps and band-offsets, to produce metal-insulator-insulator-metal (MIIM) devices. Very recent work has shown that insulator heterojunctions can be used to produce asymmetric I-V behavior in symmetric metal electrode $M_1I_1I_2M_1$ diodes.[16–18] It has not been shown whether a bilayer insulator tunnel barrier can be combined with asymmetric workfunction metal electrodes to produce $M_1I_1I_2M_2$ diodes with superior I-V asymmetry. In addition, whereas asymmetry due to resonant tunneling has been studied, asymmetry due to step tunneling, a step reduction in tunnel distance in a bilayer insulator tunnel barrier, has not yet been experimentally demonstrated. In this work, we investigate the combined effect of bilayer tunnel barriers and asymmetric electrodes in $M_1I_1I_2M_2$ tunnel diodes.

Much previous work on MIM diodes has focused on native oxides of rough polycrystalline metals.[1–7,14,16,18,19] We recently showed that roughness at the bottom metal-insulator interface can dominate the I-V behavior of MIM diodes and that the use of atomically smooth bottom electrodes combined with high quality insulators deposited via atomic layer deposition (ALD) allowed for fabrication of high quality MIM diodes with well controlled quantum mechanical tunneling.[20,21] Therefore, we fabricate M_1IIM_2 diodes using smooth amorphous metal ZrCuAlNi (ZCAN) bottom electrodes[22] and nanolaminate insulator bilayers of HfO_2 and Al_2O_3 deposited via ALD. We demonstrate that bilayer insulator tunnel barriers enable tuning of the current vs. voltage (I-V) asymmetry and non-linearity via a step reduction in the minimum tunnel distance at the applied bias at which tunneling may begin to occur through only the wider band-gap insulator layer. We find that I-V asymmetry and non-linearity are sensitive to the arrangement of the individual insulator layers with respect to the larger and smaller workfunction electrodes (e.g., $M_1I_1I_2M_2$ vs. $M_1I_2I_1M_2$) and that bilayer tunnel insulators can be arranged to enhance or oppose the built in asymmetry of the asymmetric workfunction electrodes.

MIM and MIIM diodes were fabricated on Si substrates capped with 100 nm of thermally grown SiO_2. A 150 nm thick ZCAN bottom electrode was deposited directly on the SiO_2 via DC magnetron sputtering using a $Zr_{40}Cu_{35}Al_{15}Ni_{10}$ metal target. ZCAN RMS and peak roughness were measured to be 0.3 nm and 3 nm, respectively. Next, thin oxide tunnel barriers were deposited via ALD using a Picosun SUNALE R-150B. Trimethylaluminum (TMA) and tetrakis (ethylmethylamino) hafnium (TDMAHf) were used as the metal precursors for Al_2O_3 and HfO_2, respectively. All ALD films were deposited at a chamber temperature of 250 °C using deionized water as the oxidant. Nanolaminate bilayer barriers were deposited in one continuous run without breaking vacuum. Finally, top electrodes were formed by evaporating Al dots ($\sim$0.8 mm^2) through a shadow mask. Insulator thickness on Si was measured with a J.A. Woollam WVASE32 spectroscopic ellipsometer using a Cauchy model. Transmission electron microscopy (TEM) images were taken on a FEI Titan 80–200 using samples prepared with a Quanta 3D Dual Beam focused ion beam. Metal workfunctions (Φ_M) were measured in air using a KP

[a)]Electronic mail: jconley@eecs.oregonstate.edu

Technology SKP5050 scanning Kelvin probe with a 2-mm tip and calibrated against a gold standard. Φ_{ZCAN} was measured to be approximately 4.8 eV. $\Delta\Phi$ ($\Phi_{ZCAN} - \Phi_{Al}$) was measured to be approximately 0.6 eV, confirmed by extraction from the slope of Fowler-Nordheim (FN) plots. I-V analysis was conducted at room temperature on a probe station in a dark box using an Agilent 4156C semiconductor parameter analyzer; the noise floor of this system is estimated to be on the order of 10^2 pA. As shown in the schematic device cross section inset in Fig. 1(a), the ZCAN bottom electrode (M_1) was always held at ground with bias applied to the Al top gate (M_2). To mitigate the impact of displacement current, all I-V curves were swept from zero bias to either the maximum positive or negative bias.

Two key figures of merit are defined to characterize the devices. First, I-V asymmetry, η, is defined as negative device current divided by positive current $|I_-/I_+|$ so that $\eta = 1$ indicates symmetric operation. Second, non-linearity, f_{NL}, is defined as (dI/dV)/(I/V). All band diagrams were simulated using the Boise State University Band Diagram program.[23] Materials' parameters used in simulations are consistent with values reported for similar ALD films: electron affinity (χ) = 1.3 eV, bandgap (E_G) = 6.4 eV, and relative dielectric constant (κ) = 7.6 for Al_2O_3; χ = 2.5 eV, E_G = 5.8 eV, and κ = 18 for HfO_2; and Φ_{Al} = 4.2 eV.

The behavior of the individual insulators was first measured in single layer MIM diodes. Shown in Fig. 1 are plots of (a) log (J) vs. V and (b) log (η) vs. V for M_1IM_2 diodes, where the bottom electrode M_1 is ZCAN, the top electrode M_2 is Al, and I is an approximately 3.5 nm or 10 nm thick single layer of either Al_2O_3 or HfO_2. As expected, the total current flow in Fig. 1(a) is a rough function of the relative barrier heights (see band diagrams shown as inset in Fig. 1(b)). In Fig. 1(a), the dominance of FN tunneling is apparent from the presence of the "knees" in the log (J)–V data at positive and negative biases, which are followed by several orders of magnitude of exponentially increasing current. Not shown, FN plots of $\ln(I/(V+\Delta\Phi)^2)$ vs. $1/(V+\Delta\Phi)$ confirm that Al_2O_3 and HfO_2 devices are dominated by FN tunneling in the post turn on regime.[13] Due to the asymmetric workfunction electrodes, the devices are expected to show asymmetry. In Fig. 1(b), it is seen that the 10 nm Al_2O_3 diode shows a maximum η (η_{max}) of approximately 1350 at 4.1 V. Although the Al_2O_3 devices show excellent η at higher biases, asymmetric operation at low voltage is desirable for many applications, including energy harvesting. As seen in Fig. 1(b), decreasing the tunnel barrier thickness to 3.5 nm resulted in decreased turn on voltages and increased current. However, η_{max} was not improved, most likely due to the increased influence of direct tunneling. Since decreasing the dielectric thickness in a single layer MIM diode does not improve asymmetry, another strategy is required.

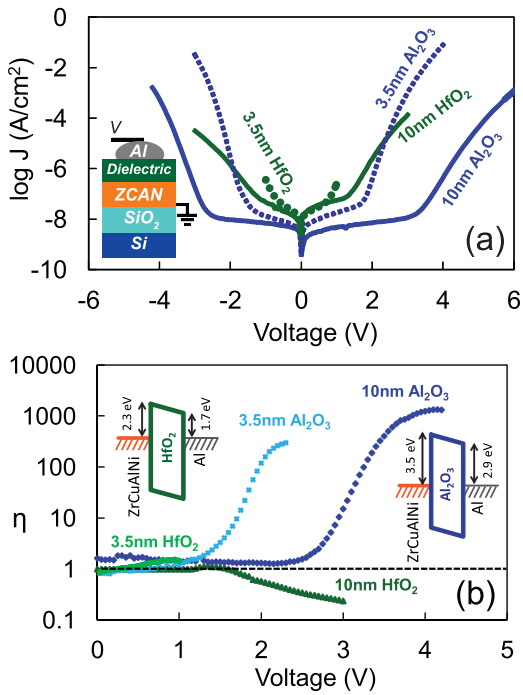

FIG. 1. Plots of (a) log (J) vs. V and (b) log(η) vs. V for single insulator MIM devices. Inset in (a) shows a schematic device cross section. Inset in (b) shows equilibrium band diagrams.

Shown in Fig. 2 are cross sectional TEM images of ZCAN/Al_2O_3/HfO_2/Al $M_1I_1I_2M_2$ devices in (a) and (c), and ZCAN/HfO_2/Al_2O_3/Al $M_1I_2I_1M_2$ devices in (b). For each insulator bilayer, 56 ALD cycles were used to deposit Al_2O_3 and 65 cycles were used to deposit HfO_2, targeting a thickness of 5 nm for each layer. The TEM images in (a) and (b) reveal that while the top insulator layer is indeed approximately 5 nm thick, in each case, the insulator layer deposited directly on the ZCAN bottom electrode is only approximately 3.5 nm thick. The reduced thickness is due to an inhibition of the ALD nucleation rate on ZCAN as compared to that on oxide. Also visible in the high resolution TEM images is the presence of an approximately 2 nm thick interfacial layer (IL) between the ZCAN and the insulator. This layer was previously determined to be composed of ZrO_x.[22] Fig. 2(c) is a lower magnification image of the device from (a), revealing the smooth nature of the ZCAN/Al_2O_3 border over an extended range. We previously found that a smooth interface is critical to achieving high yield, high quality MIM tunnel devices.[20,21]

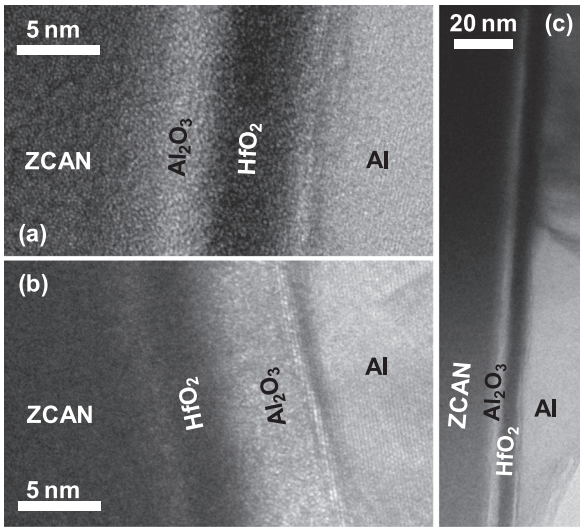

FIG. 2. Cross sectional TEM images of (a) and (c) ZCAN/Al_2O_3/HfO_2/Al $M_1I_1I_2M_2$ devices and (b) a ZCAN/HfO_2/Al_2O_3/Al $M_1I_2I_1M_2$ device. In each device, 56 ALD cycles were used to deposit Al_2O_3 and 65 cycles were used to deposit HfO_2.

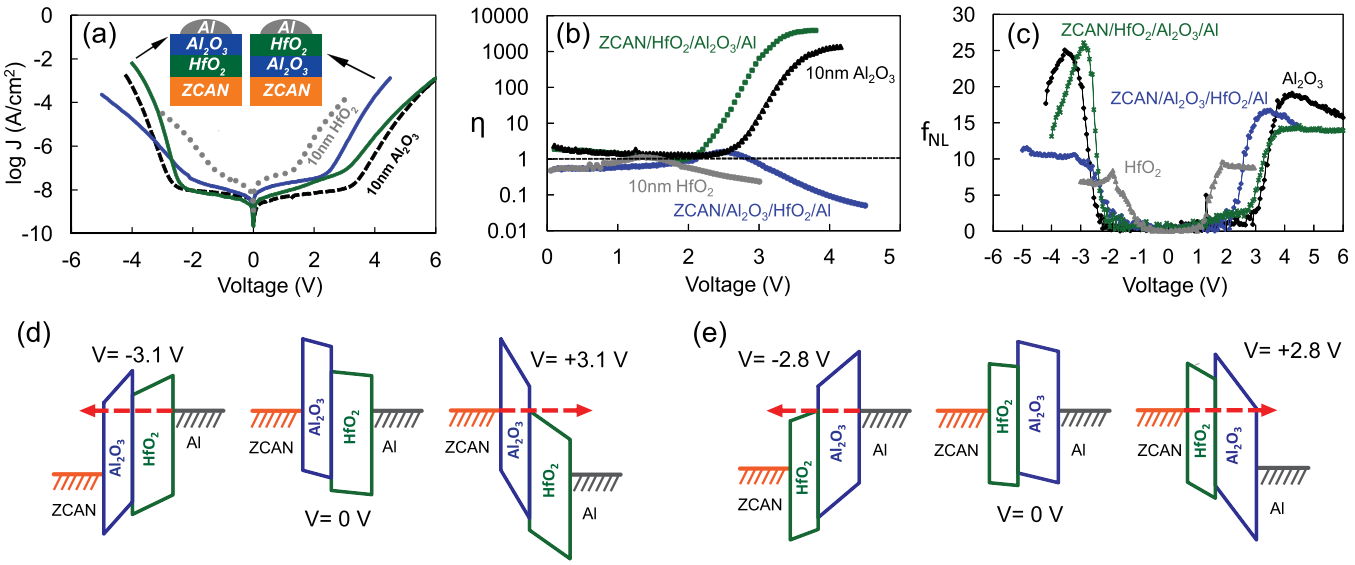

FIG. 3. Plots of (a) log (J) vs. V, (b) log (η) vs. V, and (c) f_{NL} vs. V for ZCAN/3.5 nm Al_2O_3/5 nm HfO_2/Al $M_1I_1I_2M_2$ and ZCAN/3.5 nm HfO_2/5 nm Al_2O_3/Al $M_1I_2I_1M_2$ diodes. M_1IM_2 diodes with single 10 nm layers of either Al_2O_3 or HfO_2 are included for comparison. (d) and (e) are band diagrams illustrating MIIM diodes under negative bias (left), equilibrium (center), and positive bias (right).

Shown in Fig. 3 are (a) log (J) vs. V, (b) log (η) vs. V, and (c) f_{NL} vs. V plots for ZCAN/3.5 nm Al_2O_3/5 nm HfO_2/Al $M_1I_1I_2M_2$ and ZCAN/3.5 nm HfO_2/5 nm Al_2O_3/Al $M_1I_2I_1M_2$ diodes. For reference, also shown are the 10 nm thick single insulator Al_2O_3 and HfO_2 M_1IM_2 diodes from Fig. 1. The inherent asymmetry of the bilayer insulator barriers is evident in the equilibrium band diagrams shown in Figs. 3(d) and 3(e). Differences in the I-V and η characteristics are qualitatively explained by the band diagrams, which illustrate the approximate onset of step tunneling, tunneling through only the wider band-gap Al_2O_3 layer, at positive and negative biases.

First, we consider the ZCAN/Al_2O_3/HfO_2/Al $M_1I_1I_2M_2$ device, in which the larger band-gap Al_2O_3 layer (I_1) is adjacent to the larger workfunction ZCAN electrode. Application of approximately +3.1 V (Fig. 3(d), right) should bring the Fermi level of the ZCAN to just above the conduction band of the HfO_2 so that direct tunneling may occur through only the 3.5 nm thick Al_2O_3 layer, a step reduction in the required tunnel distance. For application of an opposite polarity −3.1 V bias (Fig. 3(d), left) electrons tunneling at the Fermi level must pass through both insulating layers. A larger current is thus expected at positive bias than at an equivalent magnitude negative applied bias so that $\eta < 1$ is expected. This is observed in Fig. 3(b). Note that the polarity of the asymmetry ($\eta < 1$) is reverse that of the single Al_2O_3 layer ($\eta > 1$), indicating that the asymmetry of the bilayer insulator barrier not only *opposes* that of the built-in voltage induced by the metal workfunction asymmetry ($\Delta\Phi$) but also overwhelms its impact on device operation. Tunnel current is exponentially inversely dependent upon the barrier height ($I \propto \exp(\varphi_b^{-3/2})$).[13] Since $\varphi_{Al\text{-}HfO2} < \varphi_{ZCAN\text{-}Al2O3}$, for application of higher magnitude biases, the negative bias current will begin to increase more rapidly than the positive bias current and it is expected that the slope of the η-V plot will decrease.[13] In Fig. 3(b), it is seen that for application of 4 V bias, the slope of the η-V plot has decreased.

Next, consider the *reverse orientation* ZCAN/HfO_2/Al_2O_3/Al $M_1I_2I_1M_2$ device, in which the larger band-gap Al_2O_3 layer (I_1) is now adjacent to the smaller workfunction Al electrode. Now with −2.8 V applied to the Al gate (Fig. 3(e), left), the Fermi level in the Al gate lies just above the conduction band of the HfO_2 and electrons injected from the Al may directly tunnel through only the Al_2O_3 layer (again representing a step reduction in tunnel distance). On the other hand, for +2.8 V applied to the Al gate (Fig. 3(e), right), electrons injected from the ZCAN electrode must pass through both insulator layers. Thus, a smaller current is expected at positive bias than at an equivalent magnitude negative bias so that $\eta > 1$ is expected, again confirmed in Fig. 3(b). In this case, the asymmetry of the bilayer insulator barrier *enhances* the built-in asymmetry of the $\Delta\Phi$ and η is increased over that of the single Al_2O_3 layer M_1IM_2 diode. Note that since $\varphi_{Al\text{-}Al2O3} > \varphi_{ZCAN\text{-}HfO2}$, at higher magnitude applied biases, the current density will begin to increase more quickly under positive bias than negative bias and the slope of the η-V plot will be expected to decrease. This behavior is confirmed in Fig. 3(b).

In Fig. 3(c), it is seen that all devices exhibit excellent f_{NL} with the bilayer ZCAN/HfO_2/Al_2O_3/Al $M_1I_2I_1M_2$ diode showing the highest maximum non-linearity ($f_{NL\text{-}max} \sim 27$). This device also shows enhanced f_{NL} at low negative bias exceeding that of single layer Al_2O_3 and HfO_2 devices, consistent with its enhanced η. The reverse insulator stack orientation ZCAN/Al_2O_3/HfO_2/Al $M_1I_1I_2M_2$ device shows improved f_{NL} over the single layer Al_2O_3 M_1IM_2 diode at low positive bias and reduced f_{NL} at negative bias, consistent with the polarity of its η. Below $\sim|2\,V|$, the single layer HfO_2 device shows the best f_{NL} consistent with its lower turn-on voltage.

Shown in Fig. 4 are (a) log (J) vs. V, (b) log (η) vs. V, and (c) f_{NL} vs. V plots for *thinner* insulator bilayer ZCAN/Al_2O_3/HfO_2/Al $M_1I_1I_2M_2$ and ZCAN/HfO_2/Al_2O_3/Al $M_1I_2I_1M_2$ diodes. The HfO_2 and Al_2O_3 layers in these devices were deposited using 32 and 28 ALD cycles, respectively. The estimated thicknesses of the bottom and top insulator layers are ~1 nm and ~2.5 nm, respectively. For

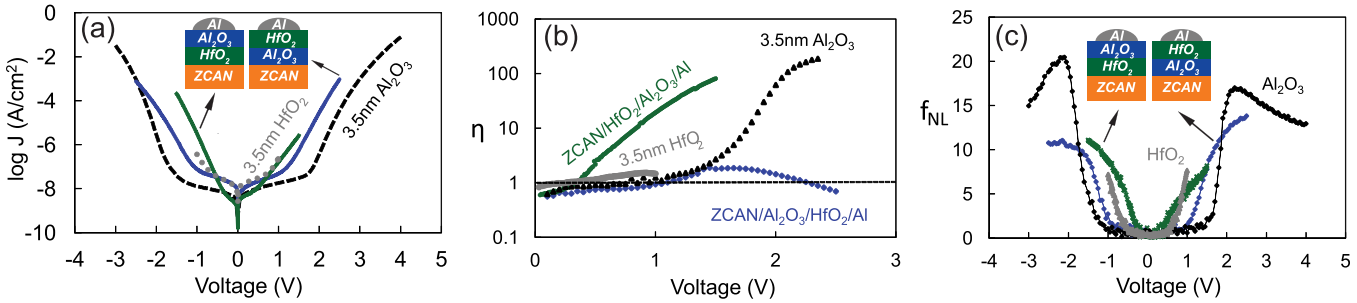

FIG. 4. Plots of (a) log (J) vs. V, (b) log (η) vs. V, and (c) f_{NL} vs. V for ZCAN/Al_2O_3/HfO_2/Al $M_1I_1I_2M_2$ and ZCAN/HfO_2/Al_2O_3/Al $M_1I_2I_1M_2$ diodes. Al_2O_3 and HfO_2 layers were deposited using 28 and 32 ALD cycles, respectively, resulting in an estimated total stack thickness of 3.5 nm. M_1IM_2 diodes with approximately 3.5 nm thick layers of either Al_2O_3 or HfO_2 are included for comparison.

reference, also plotted are the approximately 3.5 nm thick single insulator layer Al_2O_3 and HfO_2 M_1IM_2 diodes from Fig. 1, which were deposited using 56 and 65 ALD cycles, respectively. The behavior of these thinner bilayer devices is qualitatively the same as for the thicker devices. However, in all cases η_{max} is reduced, behavior that was also seen for the single layer MIM devices. Once again for the ZCAN/Al_2O_3/HfO_2/Al $M_1I_1I_2M_2$ device, the insulator bilayer *opposes* the $\Delta\Phi_M$ induced asymmetry. At voltages greater than about 2.5 V, $\eta < 1$ for the $M_1I_1I_2M_2$ device opposite to the $\eta > 1$ of the neat Al_2O_3 MIM device. For the reverse insulator orientation ZCAN/HfO_2/Al_2O_3/Al $M_1I_2I_1M_2$ device, the asymmetry induced by the $\Delta\Phi_M$ is once again *enhanced* by the bilayer insulator tunnel barrier, resulting in an η of higher magnitude than that of the neat Al_2O_3 MIM device.

As seen in Fig. 4(c), reducing the tunnel barrier thickness results in improved f_{NL} at small biases for all devices. This is due primarily to the lower turn on voltages and higher conductivity of these devices (see Fig. 4(a)). The relative improvement for the bilayer devices is even greater than for the single layer devices—as compared to single layer Al_2O_3, both of the thin MIIM devices show enhanced low bias f_{NL} for both polarities. Both MIIM devices have their highest f_{NL} for the bias polarity at which the step reduction in tunneling distance occurs. For the ZCAN/Al_2O_3/HfO_2/Al $M_1I_1I_2M_2$ devices, f_{NL} is highest at positive bias, while for ZCAN/HfO_2/Al_2O_3/Al $M_1I_2I_1M_2$ devices, f_{NL} is highest at negative bias, consistent with η data.

Overall, the thin bilayer ZCAN/HfO_2/Al_2O_3/Al device, despite reduced η_{max} and $f_{NL\text{-}max}$ as compared to the single layer Al_2O_3 device, shows excellent low voltage characteristics with $\eta > 10$ and $f_{NL} > 5$ at voltages as low as 0.8 V. For comparison, Maraghechi *et al.*[16] recently reported $\eta \sim 10$ at 3 V and $f_{NL} < 5$ at 0.8 V for a symmetric electrode Cr/2 nm HfO_2/2 nm Al_2O_3/Cr diode.

It is clear that bilayer insulators can have a significant impact on M_1IIM_2 device operation. Examining more closely the ZCAN/Al_2O_3/Al band diagram inset in Fig. 1(b) and considering asymmetry due only to tunneling based conduction, the onset of FN tunneling should be roughly at the same voltage, independent of insulator thickness. However, in Fig. 1(b), it is seen that while significant asymmetry occurs above about 3 V in the 10 nm Al_2O_3 device, significant asymmetry occurs above about 1 V in the 3.5 nm Al_2O_3 device. While part of the reason for this may be the increased thickness of the Al_2O_3 reducing conduction below the noise floor of our measurement system, another possible explanation for this discrepancy could be the thin ZrO_x IL between the ZCAN electrode and the overlying insulator (see Fig. 2 as well as Ref. 22). Because of this IL, even the nominally single layer devices might be, in fact, bilayer devices. To model the potential impact of the ZrO_x IL, band diagrams similar to those in Fig. 3(e) may be used, if HfO_2 is replaced with 2 nm of ZrO_x and an Al_2O_3 thickness of approximately either 3.5 nm or 10 nm is used. For ZCAN/2 nm ZrO_x IL/Al_2O_3/Al bilayer devices, the minimum voltage for the step reduction in tunneling distance is simulated to be approximately −2.25 V. However, in the thicker device, the electrons must tunnel through a 10 nm thick Al_2O_3 layer, while in the thinner device, the electrons tunnel through only an approximately 3.5 nm thick Al_2O_3 layer. Tunneling current is exponentially dependent upon the inverse of the barrier thickness ($I \propto \exp(1/d_{ox})$).[13] Thus, in the presence of the ZrO_x IL, the onset voltage for tunneling based asymmetry is expected to be reduced as the thickness of the Al_2O_3 layer is reduced. Looking again at the single layer Al_2O_3 devices in Fig. 1, it seems evident that I-V characteristics and η were impacted by the presence of the ZrO_x IL, although it is also possible that emission based conduction mechanisms[24] or barrier lowering in the ultrathin device structure, not considered here, may play a role. The IL layer likely plays a role in the nominally single layer HfO_2 device as well, but since the E_G and χ of HfO_2 are likely similar to the E_G and χ of the ZrO_x IL, its impact is more difficult to predict.

In conclusion, we have experimentally demonstrated that ALD nanolaminate bilayer tunnel barriers add additional asymmetry and can be used to tune I-V asymmetry and nonlinearity in asymmetric metal electrode M_1IIM_2 devices via step tunneling. I-V asymmetry and non-linearity were found to be sensitive to the arrangement of the individual insulator layers with respect to the asymmetric workfunction metal electrodes ($M_1I_1I_2M_2$ vs. $M_1I_2I_1M_2$). The bilayer insulators can be arranged to either enhance or oppose the built in asymmetric electrode workfunction induced asymmetry, depending on whether the smaller χ insulator is adjacent to the smaller or larger Φ_M electrode, respectively. By combining two methods of producing asymmetry, asymmetric metal electrodes and a bilayer insulator tunnel barrier, we were able to achieve excellent low voltage asymmetry and nonlinearity in a ZCAN/HfO_2/Al_2O_3/Al diode exceeding both that of standard single insulator layer asymmetric electrode M_1IM_2 devices as well as symmetric electrode $M_1I_1I_2M_1$

devices. It is very likely that the relative thickness of the layers in the bilayer may be used to further enhance asymmetry. These results represent clear experimental demonstration that the asymmetry and non-linearity of MIIM diodes with asymmetric workfunction electrodes can be tuned by controlling step tunneling in the bilayer insulator, thus representing an advancement in the understanding necessary to engineer thin film MIIM tunnel devices for microelectronics applications.

This work was supported in part by grants from the National Science Foundation through DMR-0805372 and CHE-1102637, the U.S. Army Research Laboratory through W911NF-07-2-0083, and the Oregon Nanoscience and Microtechnologies Institute. The authors thank B. Cowell, J. McGlone, and Professor J. F. Wager (OSU) for sputtered ZCAN films, C. Tasker for equipment support, and Dr. P. Eschbach for assistance with TEM imaging.

[1]K. Choi, F. Yesilkoy, G. Ryu, S. H. Cho, N. Goldsman, M. Dagenais, and M. Peckerar, IEEE Trans. Electron Devices **58**(10), 3519 (2011).
[2]M. Bareiß, A. Hochmeister, G. Jegert, U. Zschieschang, H. Klauk, R. Huber, D. Grundler, W. Porod, B. Fabel, G. Scarpa, and P. Lugli, J. Appl. Phys. **110**, 044316 (2011).
[3]J. A. Bean, A. Weeks, and G. D. Boreman, IEEE J. Quantum Electron. **47**(1), 126 (2011).
[4]P. C. D. Hobbs, R. B. Laibowitz, F. R. Libsch, N. C. LaBianca, and P. P. Chiniwalla, Opt. Express **15**(25), 16376 (2007).
[5]S. Krishnan, E. Stefanakos, and S. Bhansali, Thin Solid Films **516**(8), 2244 (2008).
[6]P. C. D. Hobbs, R. B. Laibowitz, and F. R. Libsch, Appl. Opt. **44**(32), 6813 (2005).
[7]S. Grover and G. Moddel, IEEE J. Photovoltaics **1**(1), 78 (2011).
[8]B. Berland, Final Report No. NREL SR-520-33263, 2003.
[9]R. Corkish, M. A. Green, and T. Puzzer, Sol. Energy **73**(6), 395 (2002).
[10]S. Vaziri, G. Lupina, C. Henkel, A. D. Smith, M. Ostlling, J. Dabrowski, G. Lippert, W. Mehr, and M. C. Lemme, "A Graphene-Based Hot Electron Transistor," Nano Lett. (2013).
[11]W. den Boer, *Active Matrix Liquid Crystal Displays* (Elsevier, Amsterdam, 2005), pp. 43–47.
[12]R. H. Reuss, B. R. Chalamala, A. Moussessian, M. G. Kane, A. Kumar, D. C. Zhang, J. A. Rogers, M. Hatalis, D. Temple, G. Moddel *et al.*, Proc. IEEE **93**(7), 1239 (2005).
[13]J. G. Simmons, J. Appl. Phys. **34**(9), 2581 (1963).
[14]P. Periasamy, J. J. Berry, A. A. Dameron, J. D. Bergeson, D. S. Ginley, R. P. O'Hayre, and P. A. Parilla, Adv. Mater. **23**(7), 3080 (2011).
[15]H. Kroemer, Phys. Scr. **T68**, 10 (1996).
[16]P. Maraghechi, A. Foroughi-Abari, K. Cadien, and A. Y. Elezzabi, Appl. Phys. Lett. **99**, 253503 (2011).
[17]S. Grover and G. Moddel, Solid-State Electron. **67**, 94 (2012).
[18]P. Maraghechi, A. Foroughi-Abari, K. Cadien, and A. Y. Elezzabi, Appl. Phys. Lett. **100**, 113503 (2012).
[19]E. N. Grossman, T. E. Harvey, and C. D. Reintsema, J. Appl. Phys. **91**(12), 10134 (2002).
[20]N. Alimardani, E. W. Cowell III, J. F. Wager, J. F. Conley, Jr., D. R. Evans, M. Chin, S. J. Kilpatrick, and M. Dubey, J. Vac. Sci. Technol. A **30**(1), 01A113 (2012).
[21]N. Alimardani, J. F. Conley, Jr., E. W. Cowell III, J. F. Wager, M. Chin, S. Kilpatrick, and M. Dubey, in *IEEE International Integrated Reliability Workshop (IRW) Final Report* (2010), pp. 80–84.
[22]E. W. Cowell III, N. Alimardani, C. C. Knutson, J. F. Conley, Jr., D. A. Keszler, B. J. Gibbons, and J. F. Wager, Adv. Mater. **23**(1), 74 (2011).
[23]R. G. Southwick III, A. Sup, A. Jain, and W. B. Knowlton, IEEE Trans. Device Mater. Reliab. **11**(2), 236 (2011).
[24]T. O'Regan, M. Chin, C. Tan, and A. Birdwell, Report No. ARL-TN-0464, December 2011.